

The Origin of Fluorine: Abundances in AGB Carbon Stars Revisited

C. Abia¹, K. Cunha², S. Cristallo^{3,4}, and P. de Laverny⁵

¹ Dpto. Física Teórica y del Cosmos, Universidad de Granada, 18071 Granada, Spain e-mail: cabia@ugr.es

² Observatório Nacional, Rua General José Cristino, 77, 20921-400 São Critovão, Rio de Janeiro, RJ, Brazil

³ INAF, Osservatorio Astronomico di Collurania, 64100 Teramo, Italy

⁴ INFN Sezione Napoli, Napoli, Italy

⁵ Laboratoire Lagrange, Université Côte d'Azur, Observatoire de la Côte d'Azur, CNRS, CS 34229, 06304 Nice cedex 4, France

Received ; accepted

ABSTRACT

Context. Revised spectroscopic parameters for the HF molecule and a new CN line list in the 2.3 μm region have been recently available, allowing a revision of the F content in AGB stars.

Aims. AGB carbon stars are the only observationally confirmed sources of fluorine. Nowadays there is not a consensus on the relevance of AGB stars in its Galactic chemical evolution. The aim of this article is to better constrain the contribution of these stars with a more accurate estimate of their fluorine abundances.

Methods. Using new spectroscopic tools and LTE spectral synthesis, we redetermine fluorine abundances from several HF lines in the K-band in a sample of Galactic and extragalactic AGB carbon stars of spectral types N, J and SC spanning a wide range of metallicities.

Results. On average, the new derived fluorine abundances are systematically lower by 0.33 dex with respect to previous determinations. This may derive from a combination of the lower excitation energies of the HF lines and the larger macroturbulence parameters used here as well as from the new adopted CN line list. Yet, theoretical nucleosynthesis models in AGB stars agree with the new fluorine determinations at solar metallicities. At low metallicities, an agreement between theory and observations can be found by handling in a different way the radiative/convective interface at the base of the convective envelope.

Conclusions. New fluorine spectroscopic measurements agree with theoretical models at low and at solar metallicity. Despite this, complementary sources are needed to explain its observed abundance in the solar neighbourhood.

Key words. stars: AGB and post-AGB; stars: abundances; Physical data and processes: nuclear reactions, nucleosynthesis, abundances

1. Introduction

Fluorine has only one stable isotope, ^{19}F , yet fragile and easily destroyed in stellar interiors by proton, neutron and alpha particle capture reactions. Major fluorine destruction channels are $^{19}\text{F}(p, \alpha)^{16}\text{O}$ and $^{19}\text{F}(\alpha, p)^{22}\text{Ne}$ reactions. Thus, any production mechanism has also to enable ^{19}F to escape from the hot stellar interiors after its production. This makes fluorine a useful tracer of the physical conditions prevailing in stellar interiors. Fluorine is thought to be produced in several scenarios: (i) Gravitational supernovae through the neutrino spallation process, (ii) low and intermediate mass ($M \leq 7 M_{\odot}$) Asymptotic Giant Branch (AGB) stars¹ during the He-burning Thermal Pulses (TP) and the subsequent Third Dredge Up (TDU) episodes, (iii) Wolf-Rayet (WR) stars in the hydrostatic He-burning phase and, even, (iv) during white dwarfs mergers (see e.g. Woosley et al. 1990; Forestini et al. 1992; Meynet & Arnould 2000; Longland et al. 2011). To date, proofs of their production have been found in AGB stars only (e.g. Jorissen et al. 1992; Werner et al. 2005; Otsuka et al. 2008; Abia et al. 2010; Lucatello et al. 2011). The origin of this element is therefore still rather uncertain and con-

tributions from the above mentioned sources seem to be necessary when comparing Galactic Chemical Evolution (GCE) model predictions (Renda et al. 2004; Kobayashi et al. 2011) to the evolution inferred from observations in Galactic field dwarf and giant stars (Recio-Blanco et al. 2012; Jönsson et al. 2014a).

To determine the relative role of the above proposed sources of fluorine, in particular of AGB stars, accurate determinations of F abundances are needed. Fluorine abundances are usually determined in cool dwarfs and giants from ro-vibrational HF lines at 2.3 μm . This spectral region, unfortunately, is placed in a region with a lot of telluric lines that can be difficult to be removed. This prevents, in many cases, the use of several HF lines to determine the F abundance in a given star. The most used one is the R9 λ 2.3358 μm HF line, which is marginally affected by blends and telluric lines (Abia et al. 2009; de Laverny & Recio-Blanco 2013). Jorissen et al. (1992) firstly used this and other secondary HF lines to derive F abundances in AGB stars of both oxygen- and carbon-rich types² showing indeed that AGB stars present large fluorine enhancements. Most recently, Abia et al. (2009, 2010) revisited this pioneering analysis using a new grid of atmosphere models for AGB carbon stars and an up-dated molecular and atomic line lists in the 2.3 μm region. Yet, they found significant F enhancements but systematically lower than those in Jorissen et al. (1992). Nevertheless, the new F enhancements are in a global agreement with nucle-

¹ In the following, we define Low Mass Stars (LMS) to be those with initial masses between about 0.8 and 2.5 M_{\odot} which experience He ignition under degenerate conditions. Stars more massive than this succeed in igniting He gently but they are not sufficiently massive to ignite C in their core. We named these Intermediate Mass Stars (IMS) having initial masses about 2.5-7 M_{\odot} .

² AGB carbon stars are those with surface C/O > 1 (by number).

osynthesis calculations of low mass AGB stars with near solar metallicity (Cristallo et al. 2011), although at lower metallicities models predict larger enhancements than observed (Abia et al. 2011; Lucatello et al. 2011). The mentioned abundance analyses in AGB stars, however, were performed using HF line excitation energies inconsistent with the partition functions adopted in the spectral synthesis. In fact, Abia et al. (2009, 2010, 2011) used the *Turbospectrum* v10.2 radiative transfer code (Plez 2012), which adopts partition functions from Sauval & Tatum (1984). However, the HF line excitation energies used in those works were from Jorissen et al. (1992) (in turn from Tipping, private communication), which are 0.25 eV higher than the correct values if using the Sauval & Tatum (1984)'s partition functions. As mentioned by Jönsson et al. (2014b), the 0.25 eV different adopted excitation energies comes from the fact that the Tipping-list uses the dissociation energy of the energy potential, and not, like Sauval & Tatum (1984), the true energy required for dissociation. The former is higher due to the zero point of the energy of the lowest vibrational level. The difference is exactly 0.25 eV for HF (Zemke et al. 1991). Recently, Jönsson et al. (2014b) presented a complete and comprehensive calculation of the excitation energies and transition probabilities for the HF molecule in the K- and L-bands. The computed HF molecular parameters agree nicely with the new list of experimental molecular parameters delivered by the HITRAN database (see Rothman et al. 2013, for details on this database). As a consequence and according to the simple curve of growth, F abundances derived with consistent partition functions would be lower by an amount $\sim \theta \Delta\chi$, where $\theta = 5040/T_{eff}$ and $\Delta\chi = 0.25$ eV.

Very recently, a new solar F abundance has been determined from the analysis of a sunspot spectrum (Maiorca et al. 2014). The new solar abundance, $\log \epsilon(F) = 4.40 \pm 0.25^3$, is significantly lower than the previous commonly adopted value 4.56 ± 0.30 although in agreement within the error bars (Asplund et al. 2009), and it is in a very good agreement with the meteoritic value, 4.46 ± 0.06 (Lodders et al. 2009). Finally, a new CN line list has been provided that might affect the fluorine abundance determination in carbon-rich stars from HF lines in the $2.3 \mu\text{m}$ region (Hedrosa et al. 2013). As a consequence, in light of the new molecular parameters and solar fluorine abundance, a re-determination of fluorine abundances in AGB stars is needed to evaluate their actual contribution to the Galactic fluorine inventory. This is the aim of the present work.

In Section 2, we describe the observations and the new spectroscopic tools used for the re-determination of the fluorine abundances in AGB carbon stars. Section 3 shows our results, while we present our conclusions in Section 4.

2. Analysis and Results

The stars studied here are the same than those analysed in Abia et al. (2010) and Abia et al. (2011) corresponding to Galactic and extragalactic AGB carbon star samples, respectively (thereafter Papers I and II). The extragalactic stars belong to the Carina dwarf galaxy (2 stars) and the Magellanic Clouds (2 stars in the SMC and 1 star in the LMC). Details about the observations, data reduction procedures and quality of the final spectra can be found in these previously published works. The re-determination of fluorine abundances in these stars has been made using the spectral synthesis method in LTE with the new

³ The abundances are given using the usual definition $\log \epsilon(X) = 12 + \log (X/H)$, where (X/H) is the abundance of the element X by number and $\log \epsilon(H) \equiv 12$.

version (v14.1) of the *Turbospectrum* code. Theoretical spectra were computed using the same atmospheric parameters (T_{eff} , $\log g$, $[Fe/H]^4$, and microturbulence) as in Papers I & II (see those for details), the only difference being the molecular line lists used here (however see below about changes in the microturbulence parameter). As noted before, the new HF line excitation energies from Jönsson et al. (2014b) are now consistent with the partition functions adopted in the *Turbospectrum* code. The immediate consequence of the systematically 0.25 eV lower excitation energies is that, in AGB carbon stars most of the HF lines in the $2.3 \mu\text{m}$ region are saturated ($\log (W_\lambda/\lambda) \geq -4.0$), even for moderate (Solar) fluorine abundances. This makes the HF lines more sensitive to the microturbulence parameter (see **Figure 1**) and, as a consequence, the total uncertainty in the derived F abundances would be larger. **For instance a change in the microturbulence by $\pm 0.2 \text{ km s}^{-1}$ may change the F abundance derived up to ± 0.15 dex.**

Updates in the molecular line lists in the $2.3 \mu\text{m}$ region has been made. In particular, we have included the contribution from the HCN molecule ($H^{12}CN/H^{13}CN$) according to the computations by Harris et al. (2003). We corrected also the wavelengths and intensities of some H_2O and OH lines in this spectral region following the new HITRAN database release. Nevertheless, due to the carbon-rich nature of our stars, the contribution to the global spectrum of these two later molecules is minimal. This is not the case, however, for the HCN molecule, which has some contribution by introducing a global extra-absorption (*veil*) that might diminish the spectral continuum up to $\sim 2 - 3\%$. Also, a significant change with respect to the line lists used in previous works is the updated CN line list in this spectral region. Details on how this CN list was computed can be found in Hedrosa et al. (2013). The new CN line list has an impact on the global fitting of the observed spectra: theoretical fits are improved for most of the stars. For several stars, the C/O ratio corresponding to the best fit to the observed spectrum needed to be revised when compared to the derived value in Papers I & II (compare Table 1 in these works with Table 2 here). Also, for the stars R Lep and SS Vir in Paper I we could not obtain a good fit to their spectra and, thus, were discarded from the analysis. On the contrary, we find now a good global fit to the spectrum of the extragalactic carbon star LMC TRM88 and determine its F abundance (previously we had just derived an upper limit F abundance for this star, see Table 1 in Paper II). The new CN line list also affects the HF lines in different ways: while the R9 line still remains almost unblended, the R22, R17 and R16 HF lines, which were used in Abia et al. (2010) (see their Table 2), are now quite blended with CN features (see **Figure 1**) and have to be considered as secondary F abundance indicators. On the contrary, the R23, R15 and R14 HF lines show less blending than before with CN lines and complement the R9 line as main fluorine indicators.

Figure 1 shows examples of synthetic fits compared to observed spectra of the stars TX Psc and UU Aur. It can be clearly appreciated the impact of the new excitation energies of the HF lines, micro- and macroturbulence parameters and that of the new CN line list used in the $2.3 \mu\text{m}$ region on the derivation of the F abundance.

2.1. The Fluorine Abundance in the Sun and Arcturus

Solar abundances are used as a zero-point for all the abundance studies. Also, Arcturus is a benchmark star in abundance analy-

⁴ We use the abundance ratio definition $[X/Y] = \log (X/Y)_* - \log (X/Y)_\odot$.

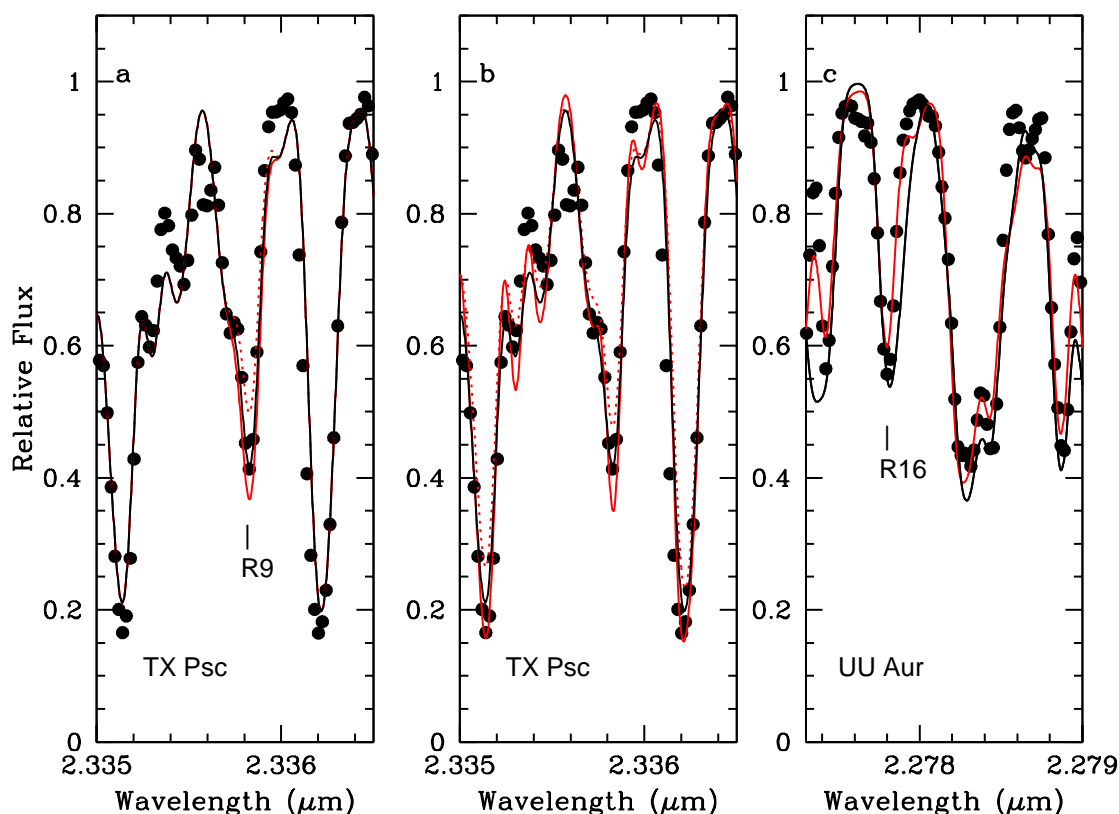


Fig. 1. Examples of synthetic fits (continuous and dotted lines) to the observed spectra (dots) for typical AGB carbon stars in the region of some HF lines: a) Left. Black line is the best fit to the R9 HF line in TX Psc ($\log \epsilon(\text{F}) = 4.7$, $\xi = 2.2 \text{ km s}^{-1}$ and $\Gamma = 13 \text{ km s}^{-1}$); red line is a fit assuming a 0.45 dex larger F abundance to show the effect of a F abundance variation similar to the total error estimated on $[\text{F}/\text{H}]$ (see text), while dotted red line shows the corresponding synthetic spectrum adopting the previously wrong lower excitation energy for this line, $\chi = 0.48 \text{ eV}$. b) Center. Black line the same as case a; red line is a synthetic spectrum adopting a lower macroturbulence parameter $\Gamma = 11 \text{ km s}^{-1}$, and dotted red line adopting a lower microturbulence, $\xi = 1.8 \text{ km s}^{-1}$ than in case a, respectively. c) Right. Effect of the new CN line list used in this work (black line) compared with the older one (red line) on the fit to the R16 HF line at $\lambda \sim 2.2778 \mu\text{m}$ in the carbon star UU Aur.

ses of cool giants. To make this analysis as consistent as possible, we redetermined the F abundance in these two reference stars using the above new molecular parameters and line lists. For the Sun, we used the sunspot Umbra Spectra in the region 1.16 to $2.5 \mu\text{m}$ by Wallace et al. (2001), and followed the same procedure as in Maiorca et al. (2014) to estimate the effective temperature of the atmospheric model that is most compatible with the sunspot umbra spectrum. We used weak and moderate intensity OH lines at $1.5 \mu\text{m}$ together with some CO lines at $2.3 \mu\text{m}$. Atomic lines of the metals present in these spectral regions cannot be used for this purpose since most of them are affected by Zeeman splitting. This is not the case for the CO and OH molecular lines, nor for the HF lines, because the corresponding vibro-rotational transitions have no spin nor orbital momentum, which means a very weak coupling between the rotational momentum and magnetic field. In fact, by using a simple Milne atmosphere model

and a vertical magnetic field, we checked that these molecular lines would be affected by Zeeman splitting only for magnetic fields larger than $\sim 10^6 \text{ G}$, an intensity much larger than that observed in the sunspots. We estimated a value $T_{\text{eff}} = 3800 \text{ K}$ from the best fit to the CO and OH lines in the sunspot spectrum. Thus we used a MARCS model atmosphere with parameters $T_{\text{eff}}/\log g/[\text{Fe}/\text{H}] = 3800/4.44/0.0$ interpolated from a grid of atmosphere models (Gustafsson et al. 2008)⁵. Similarly

⁵ We checked this approach by using a more realistic model atmosphere (Collados et al. 1994) for a sunspot which consider the effect of magnetic pressure. This sunspot umbra model atmosphere is obtained by analyzing Stokes I and V of several spectral lines. With the coolest model atmosphere ($T \sim 3900 \text{ K}$, $B = 2750 \text{ G}$ at $\log \tau_{5000} = 0.0$) deduced by these authors (see their Table 4), which resembles the MARCS model adopted here, we obtain a similar fit to

to Maiorca et al. (2014) we found that the cores of the stronger CO and of some OH lines were not so well matched. This difficulty has already been reported in the analysis of the infrared spectra of many K giants with T_{eff} similar to that we estimated in the sunspot (e.g. Ryde et al. 2002; Tsuji 2008, 2009) suggesting that the CO fundamental lines cannot be interpreted with a photospheric model only. These lines show an excess absorption ($\log W_\lambda/\lambda \geq -4.75$) that is probably nonphotospheric in origin, indicating that the structure of the hydrostatic atmosphere does not describe properly that of the sunspots⁶. Maiorca et al. (2014) arrived at the same conclusion, nevertheless they estimated a $T_{\text{eff}} = 4250$ K as the best value matching both the OH and CO lines in the sunspot spectrum. Nevertheless, we derive $\log \epsilon(\text{F}) = 4.37 \pm 0.04$ in the Sun from 10 HF lines, in agreement with the value estimated by Maiorca et al. (2014) and with the meteoritic abundance (Lodders et al. 2009). The uncertainty on this value is mainly determined by the error in the temperature estimate of the sunspot spectrum. Maiorca et al. (2014) quoted about 0.25 dex for this error that we also adopt here. In the following we will use our derived F abundance as the reference value for the Sun.

For Arcturus, we used the electronic version of the Infrared Atlas Spectrum by Hinkle et al. (1995) and the atmosphere parameters from Ryde et al. (2009). We obtain a fluorine abundance of $\log \epsilon(\text{F}) = 3.78 \pm 0.03$ from the analysis of the R7, R9 and R12 HF lines. This value is also in excellent agreement with that obtained by Jönsson et al. (2014a) and Jönsson et al. (2014b), the later from the analysis of some HF lines at $12.2 \mu\text{m}$.

2.2. Fluorine Abundances in AGB Carbon Stars

Table 2 (second column) shows the fluorine abundances redetermined in the sample of Galactic and extragalactic AGB carbon stars of different spectral types. For each star we report the number of HF lines used (between parenthesis) and the corresponding dispersion when more than a single line was used. Table 2 also shows (third column) the difference in the F abundance derived with respect to those in Papers I & II. The mean difference is -0.33 ± 0.17 dex, i.e. the abundances derived here are on average systematically lower by this amount. Note that for many stars the reduction in the F abundance is different from that applying just the correction factor $\sim 5040/T_{\text{eff}}\Delta\chi$ (see Table 1). The reason is twofold: a) the impact of the new CN line list and, b) the use here of larger macroturbulence velocities (Γ) with respect to those used in Papers I & II. The new CN line list and partition functions affects the HF lines in a different manner depending on the actual C/O ratio and the metallicity of the star (see Table 1). The **former** effect depends on the blending of a specific HF line with CN lines (see Figure 1) being this, in any case, no larger than $\sim \pm 0.20$ dex. On the other hand, because the use of new molecular line lists (mainly CN), we realised that the $2.3 \mu\text{m}$ spectral region is better fitted using a macroturbulence parameter in the range $13 - 14 \text{ km s}^{-1}$ (see Figure 1), instead of $11 - 12 \text{ km s}^{-1}$ adopted in Papers I & II. This might increase

the CO and OH lines and also a very similar average F abundance, $\log \epsilon(\text{F}) = 4.38 \pm 0.04$ (see above). This implies that magnetic pressure in a typical sunspot does not affect significantly the derivation of the F abundance.

⁶ Nevertheless, it is possible to fit reasonably well the cores of these molecular lines by extending the atmosphere model up to $\log \tau_{5000} \sim -6$. This extension of the photosphere does not affect at all the HF lines, which indicates that these lines form into deeper layers where the structure of our model atmosphere for the sunspot would be more realistic (see e.g. Tsuji 2009, for alternative solutions).

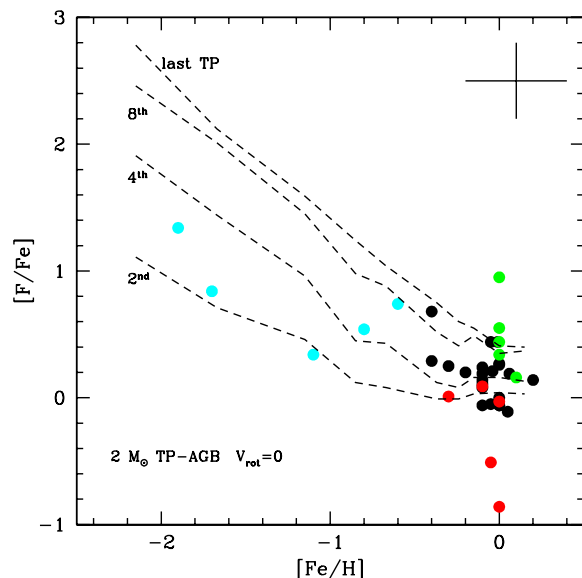


Fig. 2. $[\text{F}/\text{Fe}]$ vs. $[\text{Fe}/\text{H}]$ in the stars analysed. Circles data points are: black, N-type Galactic carbon stars; red, J-type; green, SC-type and blue, extragalactic N-type carbon stars. Dashed lines represent theoretical predictions for a non-rotating $2 M_\odot$ TP-AGB star at different TPs according to Cristallo et al. (2015b). A typical error bar is indicated.

the fluorine abundance as much as 0.25 dex, compensating partially the systematic decrease of the F abundances because of the lower χ values. In summary, the F abundances derived here differ from the previous values by an amount which is different star by star depending on the combined effect of the lower χ values, the higher Γ parameters and the blending with CN lines, **in this order of relevance.**

The total uncertainty in the abundance determination can be determined from the dependence of the fluorine abundance on the stellar atmospheric parameters; this dependence is rather similar for all the HF lines, being the uncertainty in T_{eff} , ξ , Γ and the C/O ratio the main sources of error. **A detailed discussion on the error sources and their impact in the final F abundance can be found in Abia et al. (2009). Also a discussion on the uncertainties in the derivation of the stellar metallicity $[\text{Fe}/\text{H}]$ and s -element abundances can be found in Abia et al. (2001, 2002); de Laverny et al. (2006) and Abia et al. (2008).** Concerning F, the quadratic addition of all these sources of error gives a typical uncertainty of ± 0.40 dex, together with the uncertainty of the continuum position and the dispersion in the F abundance when derived from several lines, a conservative total error would be ± 0.45 dex. This value does not include possible systematic errors as those as in the model atmospheres structure and/or N-LTE effects. However, the uncertainty in the abundance ratio between F and any other element would be lower than this value, since some of the above uncertainties cancel out when deriving the abundance ratio. Note, however, that the new $[\text{F}/\text{Fe}]$ ratios in many stars (column 5 in Table 2), do not differ significantly from the previous ones because the reduction of the solar F abundance by 0.19 dex (see previous section).

3. Discussion

The main consequence of the redetermined F abundances is that they are systematically lower than those in previous determinations, in particular for carbon stars of near solar metallicity. As it

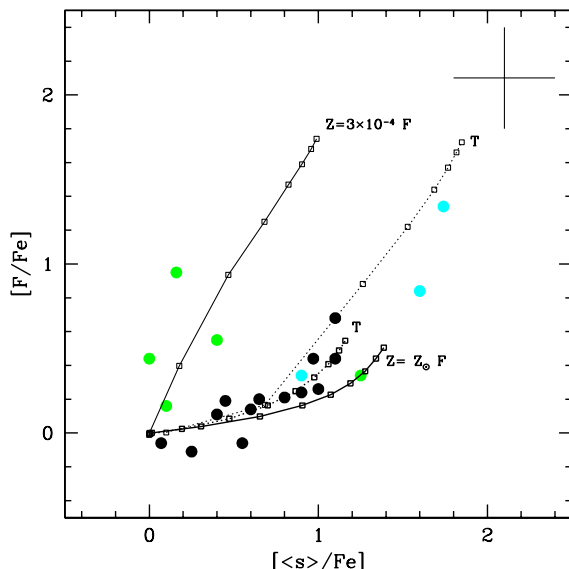


Fig. 3. Observed fluorine vs. average s-element enhancements compared with theoretical predictions. Circles symbols are as in Figure 2. Solid lines are the predictions for a non-rotating $2 M_{\odot}$ TP-AGB with metallicities (labelled) mimicking those of our stellar sample according assuming the standard ^{13}C -pocket according to Cristallo et al. (2015b) (labelled with *F*, FRUITY). Dotted lines is the prediction for a non-rotating $1.3 M_{\odot}$ metal-poor model for the same metallicities in the hypothesis of a larger ^{13}C -pocket (labelled with *T*, Tail) (see text). Small open squares in these lines mark the values predicted at different TPs. J-type AGB carbon stars have been excluded because they usually do not show s-element enhancements (Abia & Isern 2000). Typical uncertainties are shown. See text for details.

can be seen in Table 2, normal (N-type) carbon stars show only moderate F enhancements ($[\text{F}/\text{Fe}]$); the largest enhancements are now close to ~ 1 dex but are observed only in one SC-type star (WZ Cas) and some of the metal-poor N-type stars in Carina and the Magellanic Clouds. On the other hand, J-type carbon stars show no F enhancements or, in some cases, even depletions (RY Dra and Y Cvn, see Table 2). We confirm, therefore, the results of Paper I concerning the $[\text{F}/\text{Fe}]$ ratios in AGB carbon stars of different spectral types. These new enhancements can still be accounted for by current low-mass TP-AGB nucleosynthesis models (see below).

We compare the revised F abundances with theoretical models computed with the FUNS evolutionary code (Straniero et al. 2006; Cristallo et al. 2009). Those models are available on line on the web pages of the FRUITY⁷ database, which includes stars with initial masses $1.3 \leq M/M_{\odot} \leq 6.0$ and metallicities $-2.15 \leq [\text{Fe}/\text{H}] \leq +0.15$ (Cristallo et al. 2011, 2015b). Those models are calculated by coupling the physical evolution of the structure with a nuclear network including all chemical species, from hydrogen up to Pb-Bi (at the termination of the s-process path). Thus, no post process techniques are used. In FRUITY models, a thin ^{13}C pocket forms after each TDU episode. The mass extension of the pockets decreases along the AGB, thus making the first pockets the most significant for the on-going s-process nucleosynthesis. The mass-loss rate is calibrated on the observed mass loss - period relation found in Galactic AGB stars (see Straniero et al. 2006, and references therein). In order to properly follow the physical be-

haviour of the most external layers, low temperature C and N enhanced molecular opacities are used (Cristallo et al. 2007). In fact, if the convective envelope becomes C-rich (i.e. $\text{C}/\text{O} > 1$), C-bearing molecules form largely contributing to the opacity (more than O-bearing molecules). Thus, the structure becomes more opaque to photons and the external layers expand and cool. This implies an increased mass-loss rate. Note that, with respect to previously published FRUITY low mass AGB star yields (Cristallo et al. 2011), we find lower F surface abundances due to a revision in the opacity treatment of the sub-atmospheric region (Cristallo et al. 2015b). **We confirm previous calculations (Lugaro et al. 2004; Karakas 2010) showing that the stellar mass range for F production peaks around $1.5\text{--}2.5 M_{\odot}$ for all Z , showing a small dependence on the metallicity. This implies that very large surface $[\text{F}/\text{Fe}]$ ratios are predicted for decreasing metallicities. Net fluorine yields from IMS stars are lower than their low mass counterparts, but indeed have a stronger dependence on the metallicity. In fact, in our low Z IMS models the $^{19}\text{F}(p, \alpha)^{16}\text{O}$ and $^{19}\text{F}(\alpha, p)^{22}\text{Ne}$ reactions are more efficiently activated, both leading to a net fluorine destruction. In any case, however, the IMS contribution to the fluorine is negligible, due to the fact that these stars experience a definitely less efficient TDU (see Cristallo et al. 2015b).**

Figure 2 shows the $[\text{F}/\text{Fe}]$ ratios derived in our stars versus the stellar metallicity. The different dots refer to the different spectral types carbon stars in the Galaxy (see figure caption). Blue dots are the extragalactic metal-poor carbon stars belonging to the satellite galaxies. From this figure it is evident that J-type stars tend to be F-poor objects compared to the normal N-type (black dots) carbon stars. Moreover, there is a hint that SC-type stars show, on average, larger F enhancements with respect to N-type stars. With the present analysis we confirm what we found in Paper I in this respect. Note that the origin of SC- and J-type stars is still unknown. There is evidence that they are outside the classical spectral evolution M-MS-S-C(N) along the AGB phase, which is thought to be a consequence of the progressive carbon enrichment of the stellar envelope because of TDU episodes⁸. Nevertheless, the small number of J- and SC-type stars studied prevent us to reach a definite conclusion. We notice from Fig. 1 that Galactic N-type stars with slightly lower $[\text{Fe}/\text{H}]$ present larger $[\text{F}/\text{Fe}]$. This trend is confirmed for the extragalactic AGB carbon stars (blue dots), which show definitely larger fluorine overabundances, thus confirming the results of Paper II. Dashed lines in Figure 2 are the predicted $[\text{F}/\text{Fe}]$ ratios as a function of the metallicity for a typical non-rotating $2 M_{\odot}$ AGB star at different TPs (as labelled). It can be seen that observed and predicted $[\text{F}/\text{Fe}]$ ratios agree well within observational errors. Furthermore, the predicted C/O ratios in the envelope at the observed metallicity of the stars agree with the corresponding observed F enhancement. For instance, in the **FRUITY database** models with $[\text{Fe}/\text{H}] \sim 0.0, -1.1, -2.1$ (or $Z = 0.014, 10^{-3}$ and 10^{-4} , respectively) at the 3rd TP, the predicted ratios are C/O $\sim 1.1, 2.0$ and 15 , respectively. These C/O ratios are compatible with those measured in our sample at those metallicities (see Table 2). In brief, we confirm here the predicted dependence of the F production with the metallicity (e.g. Lugaro et al. 2004; Cristallo et al. 2011; Fishlock et al. 2014).

A correlation between the F and the s-element overabundance is expected if a large enough ^{13}C pocket forms after each TDU episode. This correlation comes from the ^{15}N pro-

⁸ For a detailed discussion of the properties and possible evolutionary status of SC- and J-type carbon stars see Wallerstein & Knapp (1998) and Abia et al. (2003).

⁷ <http://fruity.iaa-teramo.inaf.it>.

duction in the radiative ^{13}C pocket, the site where the s-process main component is built up (see Paper I for details). Figure 2 shows the new $[\text{F}/\text{Fe}]$ ratios vs. the observed average s-element enhancement (Abia et al. 2002; de Laverny et al. 2006; Abia et al. 2008). For the solar-like metallicity N-type carbon stars (black dots), F and s-element overabundances clearly correlate. Such a trend seems to hold for metal-poor extragalactic carbon stars (blue dots) as well, with the largest fluorine overabundances corresponding to the most s-process rich stars. In Figure 3 we compare observations with FRUITY models having two different (M,Z) combinations, i.e. initial mass $M = 2 M_{\odot}$ with $[\text{Fe}/\text{H}] = 0$ and $M = 1.3 M_{\odot}$ with $[\text{Fe}/\text{H}] = -1.67$. Both curves start from FDU abundances (solid curves). The two metallicities are representative of galactic and extragalactic carbon stars, respectively. At low Z we choose a lower initial mass in order to be consistent with the bolometric magnitudes of the observed stars ($-4.3 < M_{\text{bol}} < -5.3$). At solar metallicity observations (excluding most of SC stars) and theory (the two lower curves in Figure 3) agree nicely. At low Z (upper continuous line in Fig. 3), instead, we highlight a clear disagreement, the models showing too large ^{19}F abundances for a fixed s-process enrichment (see the discussion in Abia et al. 2011). A similar apparent deficiency of F abundances for a given s-element enhancement has been found also in the Galactic Carbon Enhanced Metal-Poor stars (CEMP) which are believed to have been polluted by mass-transfer from a former AGB star in a binary system (e.g. Lucatello et al. 2011). We test whether the inclusion of rotation might alleviate this problem by modifying the ^{19}F surface distributions in our models (see Piersanti et al. 2013). The main fluorine production channel starts with the neutrons released by the $^{13}\text{C}(\alpha, n)^{16}\text{O}$ reaction and proceeds through the nuclear chain $^{14}\text{N}(n, p)^{14}\text{C}(\alpha, \gamma)^{18}\text{O}(p, \alpha)^{15}\text{N}(\alpha, \gamma)^{19}\text{F}$ (see Cristallo et al. 2014, and references therein). The main effect of mixing induced by rotation is to dilute ^{14}N within the ^{13}C -pocket. Thus, more neutrons are captured by ^{14}N , feeding the nuclear path leading to ^{19}F production. This has also important consequences on the on-going s-process nucleosynthesis, which results less efficient depending on the initial rotation velocity (^{14}N is in fact the major neutron poison of the s-process). Thus, rotation leads to slightly larger fluorine surface abundances and to a definitely lower s-process efficiency. We conclude, therefore, that this physical process cannot be considered as a potential candidate to solve the fluorine discrepancy between theory and observations at low metallicities. A possible way to solve such a discrepancy is to obtain larger s-process enhancements for a fixed dredged up mass. Cristallo et al. (2015b) recently demonstrated that a different treatment of the inner boundary of the extra-mixed region at the base of the convective envelope during a TDU may lead to appreciable differences in the surface s-process distribution. In particular, those authors found that allowing the partial mixing to work below the formal Schwarzschild convective boundary down to the layer where the convective velocity is 10^{-11} times lower, a net increase of s-process abundances can be obtained. This derives from the fact that ^{13}C pockets are larger than those obtained in standard FRUITY models (in which the lower boundary is fixed at 2 pressure scale heights from the formal border of the convective envelope). In Figure 3 we report two models with the same combination of mass and metallicity as the FRUITY models already discussed, but with the aforescribed different mixing treatment at the base of the convective envelope (dotted lines in Fig. 3). At solar-like metallicity we find a slight decrease in the fluorine surface overabundances, this fact however not compromising the agreement with observations. At low Z, instead, we no-

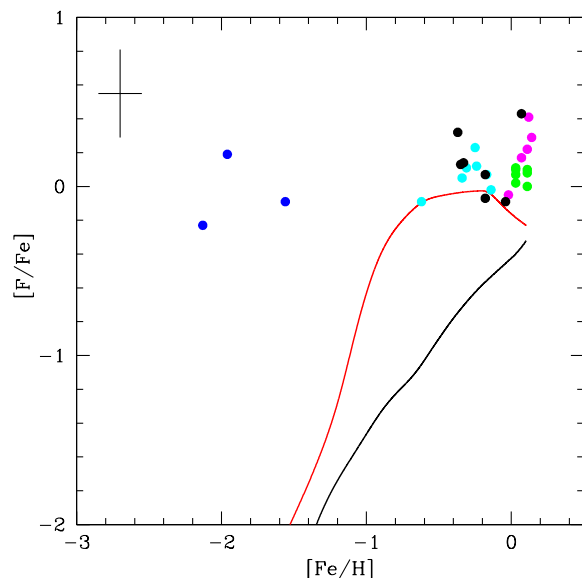


Fig. 4. $[\text{F}/\text{Fe}]$ vs. $[\text{Fe}/\text{H}]$ observed in Galactic field dwarfs and giants and open cluster stars compared with the predicted evolution from our GCE model for the solar neighbourhood including only fluorine production from AGB stars. Black line: yields from Cristallo et al. (2015a); Red line: yields from Karakas (2010). The observed ratios (circles) are from Recio-Blanco et al. (2012) (black), Li et al. (2013) (blue), Maiorca et al. (2014) (green), Jönsson et al. (2014b) (cyan) and Nault & Pilachowski (2013) (magenta). A typical error bar is shown. See text for details.

tice a large fluorine reduction for a fixed s-process surface enhancement. This leads to a reasonable fit to extra-galactic carbon stars. Thus, we conclude that larger ^{13}C pockets than those characterizing FRUITY models are needed to fit fluorine abundances in the metal-poor extra-galactic carbon stars. This further strengthens similar conclusions already reached in the study of s-process rich stars belonging to open clusters (Maiorca et al. 2012; Trippella et al. 2014) as well as in the isotopic analysis of pre-solar SiC grains (Liu et al. 2014, 2015). Note that, in any case, SC-type carbon stars marginally agree with theoretical models. However, the evolutionary status of these objects is not well understood.

3.1. The contribution of AGB stars to the fluorine abundance in the Solar neighbourhood

As mentioned in Section 1, the real contribution of AGB stars to the F inventory in the Solar neighbourhood is still a matter of debate (Jönsson et al. 2014a). The present downward revision of the F overabundances observed in AGB stars and new model predictions re-opens this issue. To shed light on this problem, we have computed a simple Galactic Chemical Evolution (GCE) model (Cristallo et al. 2015a) used recently to study the Solar System s-only distribution (i.e. of those isotopes uniquely synthesised by AGB stars). This GCE model accounts for all the constraints currently observed in the Solar neighbourhood and at the epoch of the Solar System formation (Boissier & Prantzos 1999). By using this code we have calculated the $[\text{F}/\text{Fe}]$ vs. $[\text{Fe}/\text{H}]$ evolution including only the F contribution from AGB stars. Figure 4 shows the computed evolution (black line) compared to the observed one inferred from Galactic unevolved field dwarf and giant stars **and open cluster stars** (see caption of Fig-

ure 4 for the references⁹). It is evident that the AGB contribution to F is not enough to account for the observed abundance of this element in the Solar System: the GCE model predicts a factor ~ 3 lower $[F/Fe]$ ratio than observed at $[Fe/H] \sim 0.0$. We have computed also the evolution using the F yields obtained with the STROMLO stellar evolutionary code (see e.g. Karakas 2010, red line). From Figure 4, it is evident that the GCE model produces quite different results when using different ^{19}F yield inputs. The reasons for such a discrepancy are manifold. Among the many different inputs of the two stellar codes, two main candidates can be identified: the treatment of convection and the mass-loss rate. With respect to ours models, those of Karakas (2010) show an increased TDU and hot bottom burning efficiency. While the first difference leads to larger ^{19}F surface enrichments, the second implies a more efficient fluorine destruction. However, when weighting the contribution with a typical initial mass function, the first term becomes dominant. As a consequence, the fluorine production in Karakas's stellar models is larger than our. This is particularly evident for stellar models with initial mass $M \geq 3 M_{\odot}$ at low metallicity ($Z \leq 6 \times 10^{-3}$). Another difference arises from the adopted mass-loss rate law. The models by Karakas (2010) follow the prescriptions of Vassiliadis & Wood (1993). At fixed period, our mass-loss rate is more efficient (see Figure 6 in Straniero et al. 2006). This leads to a faster erosion of the convective envelope and, thus, to lower yields. Moreover, Karakas (2010) included a metallicity dependency that we do not take into account. In any case, using the Karakas (2010) yields for F (red line), the computed evolution agrees better with the observed trend at $[Fe/H] \sim 0.0$, but the previous conclusion still holds: AGB stars alone cannot account for the current F abundance in the Solar neighbourhood and other sources of F are required to explain its observed evolution. **Note that although using the Karakas's yields one might account for the observed $[F/Fe]$ ratios at $[Fe/H] \sim -0.5$ (within the observational uncertainties, see Fig. 3), at higher metallicities her yields fail to get $[F/Fe] \sim 0.0$ as the observations seems to indicate on average.** Additional fluorine abundance determinations in dwarf and giant stars covering a wide range of metallicities would help to clarify the nature of these additional sources. We notice, furthermore, that current stellar theoretical models reproduce the ^{19}F abundances observed in AGB stars. This further strengthen the need of additional fluorine sources.

4. Summary

Fluorine abundances have been redetermined in a sample of Galactic and extragalactic AGB carbon stars using consistent partition functions and spectroscopic parameters of HF lines. A redetermination of the F abundance in the Sun and Arcturus has been also made, which agree with other recent F abundance determinations in these stars. Concerning AGB carbon stars, the new F abundances are systematically lower in average by 0.33 dex with respect to previous determinations. For a specific carbon star the difference depends on a combination between the new excitation energies of the HF lines, a higher macroturbulence parameter, and a new CN line list used here. The F abundances found in the near solar metallicity carbon stars agree with

the extant nucleosynthesis models in low-mass AGB stars. For the metal-poor AGB carbon stars belonging to several satellite galaxies, a satisfactory fit can be obtained by using theoretical models with larger ^{13}C pockets with respect to our standard FRUITY models. Using new F yields from low and intermediate-mass AGB stars and a GCE model we evaluate the contribution of these stars to the F inventory in the solar neighbourhood and conclude that additional sources of F are needed to explain the observed evolution of this element.

Acknowledgements. Part of this work was supported by the Spanish grant AYA-2011-22460. NSO/Kitt Peak FTS data used here were produced by NSF/NOAO. **We thank A. Asensio Ramos for his help on the atmosphere models for sunspots.**

References

- Abia, C., Busso, M., Gallino, R., et al. 2001, *ApJ*, 559, 1117
 Abia, C., Cunha, K., Cristallo, S., et al. 2010, *ApJ*, 715, L94
 Abia, C., Cunha, K., Cristallo, S., et al. 2011, *ApJ*, 737, L8
 Abia, C., de Laverny, P., & Wahlin, R. 2008, *A&A*, 481, 161
 Abia, C., Domínguez, I., Gallino, R., et al. 2002, *ApJ*, 579, 817
 Abia, C., Domínguez, I., Gallino, R., et al. 2003, *PASA*, 20, 314
 Abia, C. & Isern, J. 2000, *ApJ*, 536, 438
 Abia, C., Recio-Blanco, A., de Laverny, P., et al. 2009, *ApJ*, 694, 971
 Asplund, M., Grevesse, N., Sauval, A. J., & Scott, P. 2009, *ARA&A*, 47, 481
 Boissier, S. & Prantzos, N. 1999, *MNRAS*, 307, 857
 Collados, M., Martínez Pillet, V., Ruiz Cobo, B., del Toro Iniesta, J. C., & Vazquez, M. 1994, *A&A*, 291, 622
 Cristallo, S., Abia, C., Straniero, O., & Piersanti, L. 2015a, *ApJ*, 801, 53
 Cristallo, S., Di Leva, A., Imbriani, G., et al. 2014, *A&A*, 570, A46
 Cristallo, S., Piersanti, L., Straniero, O., et al. 2011, *ApJS*, 197, 17
 Cristallo, S., Straniero, O., Gallino, R., et al. 2009, *ApJ*, 696, 797
 Cristallo, S., Straniero, O., Lederer, M. T., & Aringer, B. 2007, *ApJ*, 667, 489
 Cristallo, S., Straniero, O., Piersanti, L., & Gobrecht, D. 2015b, *ArXiv e-prints* de Laverny, P., Abia, C., Domínguez, I., et al. 2006, *A&A*, 446, 1107
 de Laverny, P. & Recio-Blanco, A. 2013, *A&A*, 560, A74
 Fishlock, C. K., Karakas, A. I., Lugaro, M., & Yong, D. 2014, *ApJ*, 797, 44
 Forestini, M., Goriely, S., Jorissen, A., & Arnould, M. 1992, *A&A*, 261, 157
 Gustafsson, B., Edvardsson, B., Eriksson, K., et al. 2008, *A&A*, 486, 951
 Harris, G. J., Pavlenko, Y. V., Jones, H. R. A., & Tennyson, J. 2003, *MNRAS*, 344, 1107
 Hedrosa, R. P., Abia, C., Busso, M., et al. 2013, *ApJ*, 768, L11
 Hinkle, K., Wallace, L., & Livingston, W. 1995, *PASP*, 107, 1042
 Jönsson, H., Ryde, N., Harper, G. M., et al. 2014a, *A&A*, 564, A122
 Jönsson, H., Ryde, N., Harper, G. M., Richter, M. J., & Hinkle, K. H. 2014b, *ApJ*, 789, L41
 Jorissen, A., Smith, V. V., & Lambert, D. L. 1992, *A&A*, 261, 164
 Karakas, A. I. 2010, *MNRAS*, 403, 1413
 Kobayashi, C., Izutani, N., Karakas, A. I., et al. 2011, *ApJ*, 739, L57
 Li, H. N., Ludwig, H.-G., Caffau, E., Christlieb, N., & Zhao, G. 2013, *ApJ*, 765, 51
 Liu, N., Gallino, R., Bisterzo, S., et al. 2014, *ApJ*, 788, 163
 Liu, N., Savina, M. R., Gallino, R., et al. 2015, *ApJ*, 803, 12
 Lodders, K., Palme, H., & Gail, H.-P. 2009, *Landolt Börnstein*, 44
 Longland, R., Lorén-Aguilar, P., José, J., et al. 2011, *ApJ*, 737, L34
 Lucatello, S., Masseron, T., Johnson, J. A., Pignatari, M., & Herwig, F. 2011, *ApJ*, 729, 40
 Lugaro, M., Ugalde, C., Karakas, A. I., et al. 2004, *ApJ*, 615, 934
 Maiorca, E., Magrini, L., Busso, M., et al. 2012, *ApJ*, 747, 53
 Maiorca, E., Uitenbroek, H., Uttenhaller, S., et al. 2014, *ApJ*, 788, 149
 Meynet, G. & Arnould, M. 2000, *A&A*, 355, 176
 Nault, K. A. & Pilachowski, C. A. 2013, *AJ*, 146, 153
 Otsuka, M., Izumiura, H., Tajitsu, A., & Hyung, S. 2008, *ApJ*, 682, L105
 Plez, B. 2012, *Turbospectrum: Code for spectral synthesis*, Astrophysics Source Code Library
 Recio-Blanco, A., de Laverny, P., Worley, C., et al. 2012, *A&A*, 538, A117
 Renda, A., Fenner, Y., Gibson, B. K., et al. 2004, *MNRAS*, 354, 575
 Rothman, L. S., Gordon, I. E., Babikov, Y., et al. 2013, *J. Quant. Spec. Radiat. Transf.*, 130, 4
 Ryde, N., Edvardsson, B., Gustafsson, B., et al. 2009, *A&A*, 496, 701
 Ryde, N., Lambert, D. L., Richter, M. J., & Lacy, J. H. 2002, *ApJ*, 580, 447
 Sauval, A. J. & Tatum, J. B. 1984, *ApJS*, 56, 193
 Straniero, O., Gallino, R., & Cristallo, S. 2006, *Nuclear Physics A*, 777, 311
 Trippella, O., Busso, M., Maiorca, E., Käppeler, F., & Palmerini, S. 2014, *ApJ*, 787, 41
 Tsuji, T. 2008, *A&A*, 489, 1271
 Tsuji, T. 2009, *A&A*, 504, 543
 Vassiliadis, E. & Wood, P. R. 1993, *ApJ*, 413, 641
 Wallace, L., Hinkle, K., & Livingston, W. C. 2001, *Sunspot umbral spectra in the region 4000 to 8640 cm⁻¹ (1.16 to 2.50 [microns])*
 Wallerstein, G. & Knapp, G. R. 1998, *ARA&A*, 36, 369
 Werner, K., Rauch, T., & Kruk, J. W. 2005, *A&A*, 433, 641
 Woosley, S. E., Hartmann, D. H., Hoffman, R. D., & Haxton, W. C. 1990, *ApJ*, 356, 272
 Zemek, W. T., Stwalley, W. C., Coxon, J. A., & Hajigeorgiou, P. G. 1991, *Chemical Physics Letters*, 177, 412

⁹ All the $[F/Fe]$ ratios shown in Figure 4 have been re-scaled to the new solar F abundance according to Table 2. Note that these ratios may not differ significantly from the original ones in the mentioned papers, since apart of the lower Solar F abundance used here, one should also consider the decrease of the F abundance derived in a specific star when using the correct χ values.

Table 1. Variations (new-old) in the F abundance derived (in dex) from some HF lines due o the combined effect of the new χ 's and CN molecular list for specific atmosphere parameters

T_{eff}	$\log g$	[Fe/H]	C/O	HF lines		
				R9	R14	R15
2800	0.0	0.0	1.02	-0.40	-0.35	-0.35
3300	0.0	0.0	1.02	-0.40	-0.35	-0.35
2800	0.0	0.0	1.10	-0.40	-0.35	-0.40
2800	0.0	-1.0	1.70	-0.45	-0.45	-0.45
4000	3.0	0.0	0.58	-0.33	-0.30	-0.25
5500	4.0	0.0	0.58	-0.30	-0.30	-0.30

Notes. It is assumed [F/Fe]= 0.0, a **macroturbulence** $\Gamma = 13 \text{ kms}^{-1}$ in all the cases, and **microturbulence** $\xi = 2.2$ or 1.5 kms^{-1} , for carbon- or oxygen-rich stars, respectively.

Table 2. Fluorine Abundances and Element Ratios

Star	$\log \epsilon(\text{F})^a$	$\Delta \log \epsilon(\text{F})^b$	C/O	[Fe/H]	[F/Fe]	[<s>/Fe]
Sun	4.37±0.04(10)	0.19	0.58	0.00	0.00	0.00
Arcturus	3.78±0.02(3)	0.37	0.20	-0.53	-0.07	-0.01
N-type						
AQ Sgr	4.34±0.08 (5)	0.29	1.03	-0.10	0.08	–
BL Ori	4.62±0.20 (5)	0.30	1.04	0.00	0.26	1.00
RT Cap	4.30	0.36	1.20	0.00	-0.06	–
RV Cyg	4.30±0.00 (4)	0.40	1.09	0.00	-0.06	0.07
S Sct	4.37±0.05 (5)	0.25	1.05	-0.10	0.11	0.40
ST Cam	4.45±0.00 (4)	0.27	1.02	-0.10	0.19	0.45
TU Gem	4.63±0.24 (5)	0.29	1.07	0.00	0.27	–
TW Oph	4.26±0.06 (3)	0.35	1.12	-0.40	0.29	–
TX Psc	4.65±0.07 (6)	0.18	1.03	-0.39	0.69	1.10
U Cam	4.20±0.08 (4)	0.38	1.23	-0.10	-0.06	0.55
U Hya	4.70±0.20 (6)	0.37	1.05	-0.05	0.39	1.10
UU Aur	4.55±0.14 (7)	0.33	1.06	0.00	0.19	0.45
UX Dra	4.56±0.18 (5)	0.29	1.05	-0.20	0.20	0.65
V460 Cyg	4.47±0.12 (4)	0.18	1.07	-0.05	0.15	0.80
V Aql	4.26±0.05 (5)	0.36	1.05	-0.05	-0.05	0.20
VY UMa	4.50±0.03 (5)	0.20	1.06	-0.10	0.24	0.90
W CMa	4.68±0.13 (5)	0.27	1.07	0.20	0.12	0.60
W Ori	4.30±0.00 (3)	0.12	1.07	0.05	-0.10	0.25
X Cnc	4.32±0.08 (4)	0.61	1.03	-0.30	0.25	–
Y Hya	4.40±0.00 (2)	0.50	1.18	-0.10	0.14	–
Y Tau	4.36±0.17 (4)	0.21	1.04	0.00	0.00	0.05
Z Psc	4.80±0.06 (5)	0.10	1.08	-0.01	0.44	0.97
SC-type						
CY Cyg	4.62±0.03 (4)	0.53	1.00	0.10	0.15	0.10
FU Mon	4.91±0.07 (5)	0.24	1.00	0.00	0.55	0.40
GP Ori	4.70±0.14 (5)	0.56	1.01	0.00	0.34	1.25
RZ Peg	4.80±0.02 (7)	0.20	1.00	0.00	0.44	0.00
WZ Cas	5.31±0.14 (7)	0.49	1.01	0.00	0.95	0.16
J-type						
R Scl	4.07±0.05 (4)	0.11	1.02	-0.30	0.01	–
RY Dra	3.80	0.68	1.12	-0.05	-0.51	<0.20
T Lyr	4.32	0.35	1.14	0.00	-0.04	–
VX And	4.30±0.00 (2)	0.05	1.76	-0.10	0.04	0.2
Y Cvn	< 3.50	> 0.85	1.12	0.00	< -0.86	<0.2
ExtraGalactic N-type						
LMC TRM88	4.50	0.35	1.62	-0.60	0.74	–
SMC GM780	4.10	–	3.10	-0.80	0.53	–
SMC BMB B30	3.60	0.00	1.47	-1.10	0.34	0.90
Carina ALW6	3.50	0.20	12.0	-1.70	0.84	1.60
Carina ALW7	3.80	0.60	19.0	-1.90	1.34	1.74

Notes. [<s>/Fe] is the average s-element enhancement according to Abia & Isern (2000), Abia et al. (2002), de Laverny et al. (2006) and Abia et al. (2008).

^(a) The number in parenthesis indicates the number of HF lines used. ^(b) Abundance difference in the sense Abia et al. (2010) (Galactic stars) or Abia et al. (2011) (extragalactic stars) minus this work. In the cases of the Sun and Arcturus the differences are respect to that derived in Asplund et al. (2009) and Abia et al. (2009), respectively.